scientific reports

Check for updates

OPEN

Alkali and sulfate effects on mechanical properties and microscopic mechanisms of slag and fly ash geopolymers

Miaomiao Gong[1,2]✉, Ao Shen[1,3], Yiyi Wang[1,3], Haoran Lin[1,3] & Rui He[1,3]

Aiming at the problem that it is difficult to realize low-cost, high-performance and large-scale utilization of cementitious materials prepared from bulk solid wastes, this paper constructs a set of composite cementitious system based on alkaline activation of slag and fly ash (FA) by calcium carbide slag (CCS) and synergistic activation of sodium sulfate (Na_2SO_4) as a chemical dopant. The influence of factors such as solid waste type, mixing ratio, and Na_2SO_4 content on the mechanical properties of composite cementitious systems was investigated by assessing compressive strength and analyzing microstructure using XRD, SEM-EDS, and FTIR. The test results indicate that CCS and Na_2SO_4 exert significant influences on the strength of the composite cementitious system. CCS acts as an alkali activator, enhancing the system's hydration with an optimal dosage of 25%. Low Na_2SO_4 content also promotes hydration, but higher concentrations disrupt the internal structure of the cementitious system post-coagulation, with an optimal content of 6%. The Projection Pursuit Regression (PPR) strength prediction model can fit the actual experimental data very well, which provides a feasible method for the proportion design and mechanical strength prediction of all-solid-waste cementitious systems.

Keywords Solid wastes, Geopolymers, Alkali-sulfate synergistic activation, Mechanical property, PPR modeling

Traditional Portland cement has been widely used in the field of building materials, but its long-term use inevitably leads to a large amount of carbon dioxide emissions and energy consumption, thus exacerbating the greenhouse effect[1]. In recent years, with the introduction of the concepts of "Carbon Peaking and Carbon Neutrality[2]" and "Green Building Materials[3]", the use of solid waste has attracted the attention of researchers. Alkali-activated materials are a new type of cementitious system with pozzolanic activity that is based on silicon and aluminum as the main elements. These methods rely mainly on the introduction of alkalis (such as NaOH and sodium silicate) to cause the silicon and aluminum in the raw materials to form a polyaluminate material with a three-dimensional network structure. Because the good mechanical properties of alkali-activated materials are primarily due to silicon and aluminum rather than calcium, these materials are also referred to as geopolymers[4]. According to their chemical composition, precursors can be divided into high-calcium materials (slag) and low-calcium or calcium-free materials (fly ash, silica fume, etc.). Geopolymers have attracted the attention of many researchers because of their unique microstructural properties and excellent mechanical properties. FA has played a role in the manufacturing of geopolymers and promoted the development of environmentally friendly building materials[5]. Slag contains chemical components such as CaO and SiO_2. The silicon-rich phase C-S-H formed under the action of an activator has stronger atomic bonds and greater strength than the calcium-rich phase cementitious products formed from traditional Portland cement[6].

Strongly corrosive saline soils are widely distributed in Northwest China, and severe erosion from sulfate and other types of salt crystallization has occurred. In particular, salt lakes are widely distributed in Northwest China, and underground engineering structures have been in erosive solutions for a long time or in dry and wet cycle areas, which significantly damages and deteriorates the structure[7]. Could the idea of "turning danger into safety" have been used to convert the hazard of sulfate erosion into a way to improve the strength of geopolymers?

[1]College of Hydraulic and Civil Engineering, Xinjiang Agricultural University, Urumqi 830052, Xinjiang, People's Republic of China. [2]Xinjiang Hydraulic Engineering Geotechnical and Structural Engineering Technology Research Center, Urumqi 830052, Xinjiang, People's Republic of China. [3]Ao Shen, Yiyi Wang, Haoran Lin, Rui He ✉email: gongmiaomiao@xjau.edu.cn

Sulfate is a basic metal sulfate. As an activator, sodium sulfate is more economical and environmentally friendly than sodium hydroxide and sodium silicate are[8]. Adding sodium sulfate to the gelation system could promote the hydration reaction[9]. Some scholars have reported that the addition of sodium sulfate to the gelation material significantly affects the hydration reaction rate in the gelation system and plays a positive role[10–14]. Sodium sulfate participates in the hydration reaction, promotes the formation of the AFt phase, increases the alkalinity of the sample, and stimulates gel formation, and the hydration products fill the pores of the material, thereby optimizing the microstructure of the gelation material[15]. However, a high sodium sulfate content accelerates the production of more expansive products, destroys the microstructure of the cementitious material, and leads to a sharp decrease in strength[16,17]. Since the pH of a sulfate solution is generally between 9 and 10, the hydration of cementitious material is promoted more slowly than that of other strongly alkaline materials, and early strength often does not meet the requirements. If an alkaline material was added to a sulfate-activated cementitious material system, the early strength of the paste could be significantly improved, but the rate of increase in the late strength would be reduced[18].

As a strongly alkaline waste residue product generated in industrial production, CCS can cause serious environmental damage if it is landfilled or dumped. How to achieve the reuse of CCS has become an important issue that needs to be addressed today[19]. The comprehensive utilization and environmental management of CCS face many challenges, and further research and technological improvements are needed to increase the efficiency of its application and reduce its environmental impact.

CCS is strongly alkaline and can be used as an alkali activator to establish an alkali-activated solid waste gel system. CCS had a good activating effect on cementitious materials such as slag. The alkaline material CCS can form a stable alkaline environment, promote the initial hydration reaction[20], and provide many Ca^{2+} ions, which provide raw materials for the hydration products[21–23]. An analysis of the evolution of the mechanical strength and the development of the microstructure of the CCS alkali-activated gelling material revealed that the NaCl, $CaCl_2$ and $Ca(OH)_2$ components in the alkali residue participated in the hydration process, resulting in a denser microstructure and lower porosity, which increased the compressive strength and density[24,25].

To improve the early strength of sodium sulfate-activated geopolymer materials and ensure the late strength of the gelation system, CCS was added to the geopolymer material. Many previous studies have focused on enhancing the properties of FA/Slag-based alkali-activated materials via sulfate or CCS[26–28]. However, there has been very limited research on the combined effects of these two factors on the mechanical properties and microstructures of hydrated products in multifunctional solid waste gelation systems.

In this study, composite cementitious systems were prepared using common industrial byproducts, including CCS, FA and slag, as the primary materials. Additionally, Na_2SO_4 was added as an activator to further stimulate the gelling material. The impacts of the solid waste type, mixing ratio and Na_2SO_4 content on the mechanical properties of composite cementitious systems were examined by determining the compressive strength of each system. The microstructure was analyzed via XRD, SEM-EDS and FTIR to elucidate the mechanism of action of each component. A compressive strength prediction model of the composite cementitious system was established via PPR, thereby providing a theoretical basis for the safe and efficient utilization of industrial waste materials such as CCS, FA and slag.

Materials and methods

Raw materials

The raw materials for this study include Class I C FA from thermal power plants in Chang ji City, CCS from acetylene production at Xinjiang Hua tai Heavy Chemical Co., and S75 Slag from Xinjiang Bao Xin Sheng yuan Co. Anhydrous Na_2SO_4 (99% analytically pure) was obtained from Tianjin Zhiyuan Chemical Reagent Co., and tap water was used for testing. Table 1 presents the main chemical compositions and apparent densities of the materials used in the cementitious system. The raw material XRD spectrum was shown in Fig. 1.

Mix proportions and preparation of sample

Mix proportions

Three cementitious systems were prepared, comprising CCS-Slag (C-S), CCS-FA (C-F), and CCS-Slag-FA (C-S + F). The proportion of mixture is shown in Table 2.

Preparation of sample specimen preparation

The sample preparation process was conducted `in accordance with the JGJ/T 70-2009[29] standard, with material proportions determined based on the experimental program table. Initially, the ingredients should be weighed and subsequently blended for a duration of 30 s. Subsequently, a precise quantity of Na_2SO_4 is weighed and dissolved in distilled water to produce a salt solution. Subsequently, the prepared salt solution is introduced to the mixed ingredients, and the mixture is subjected to a 60-second period of agitation. Once mixing was

	Chemical composition of cementitious materials (%)									
	Loss	SiO_2	Al_2O_3	Fe_2O_3	CaO	MgO	SO_3	K_2O	Na_2O	Apparent density ($g{\cdot}cm^{-3}$)
CCS	22.08	4.71	1.36	0.85	69.60	0.00	0.10	0.03	0.06	0.68
FA	0.42	48.68	17.53	8.28	12.72	2.49	1.06	1.13	1.04	2.36
Slag	1.12	37.94	18.43	0.92	39.00	2.14	0.22	0.11	0.11	2.60

Table 1. Chemical composition and apparent density table of cementitious materials.

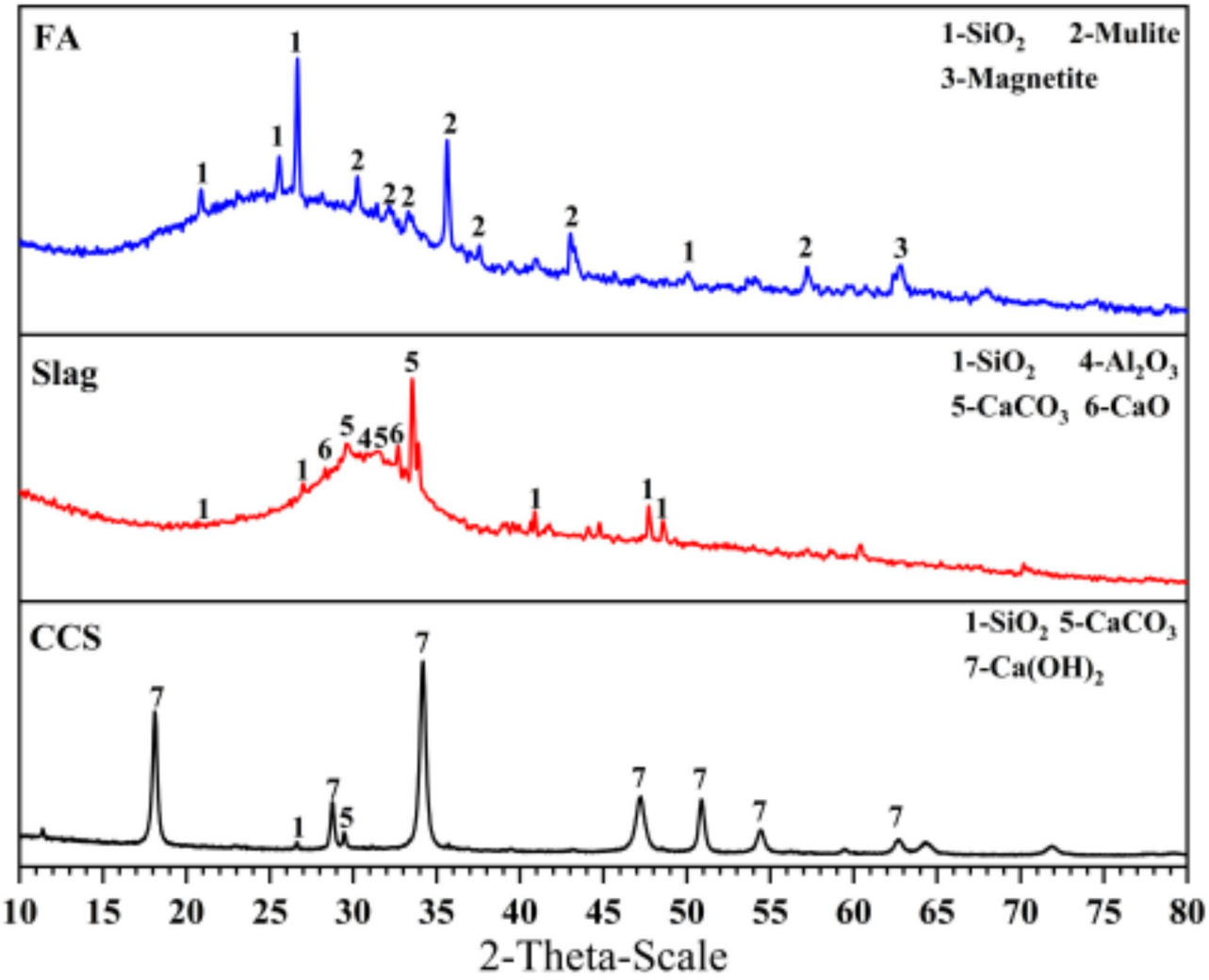

Fig. 1. XRD patterns of FA, Slag and CCS.

Cementitious system	CCS dosage (%)	FA dosage (%)	Slag dosage (%)	Na_2SO_4 content (%)	Water-cement ratio
C-S	5, 10, 15, 20, 25, 30	0	95, 90, 85, 80, 75, 70	2, 4, 6,8,10	0.35
C-F		95,90,85, 80, 75, 70	0		
C-S + F		47.5, 45, 42.5, 40, 37.5, 35	47.5, 45, 42.5, 40, 37.5, 35		

Table 2. Mix proportion of multi-component solid waste cementitious system.

complete, the slurry was poured into molds with dimensions of 40 × 40 × 160 mm. The molded specimens were subsequently placed in a standard curing box under controlled conditions (temperature of 20 ± 3 °C and humidity of 90%) for curing. After 24 h, the specimens were demolded and returned to the curing box to continue the curing process. After 28 days of curing, the specimens underwent unconfined compressive strength testing and microstructure analysis. The detailed procedure is illustrated in Fig. 2.

Test methods

Compressive strength test

Compressive strength is tested using TYA −300B automatic pressure tester. The compressive strength tests were carried out on samples with curing time of 28 days. The loading rate of the apparatus was fixed at 2400N/s ± 200N/s during the tests and each set of tests was repeated three times and the strength values used in the study were the average values calculated from the measured data.

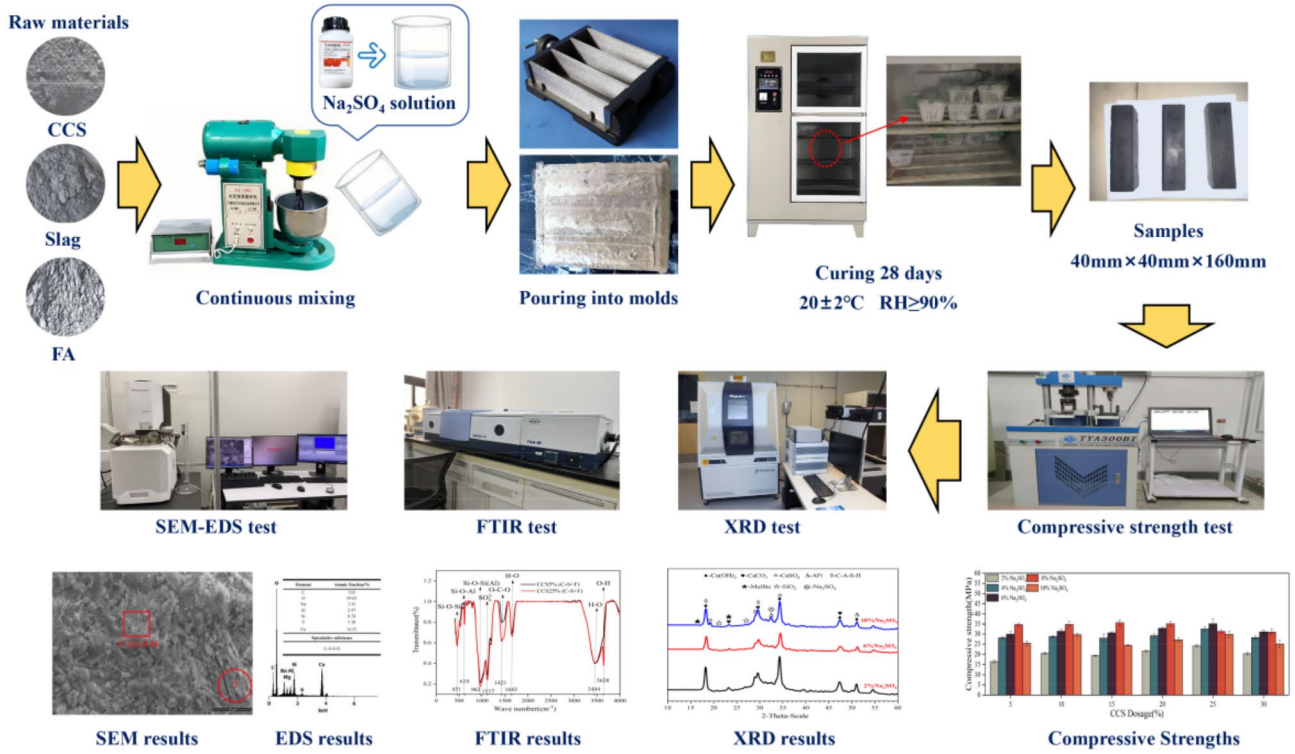

Fig. 2. Production of specimens and testing procedures flow chart.

XRD test

XRD is a technique used to identify the mineralogical composition of materials and is widely used in many studies. First, the crushed specimens after compressive strength testing were immersed in an anhydrous ethanol solution to stop their hydration reaction, and then dried in a vacuum oven at 45 °C until constant weight. Subsequently, the dried specimens were ground to a powder, sieved through a 75 μm sieve, and then the powder was filled and pressed into the grooves of the test slides for XRD testing. The XRD tests were performed using a Bruker D8 Advance X-ray Diffractometer, with the scanning range of the tests set to 10–80° 2θ and the scanning speed of the instrument set to 10°/min.

FTIR test

The test was carried out with an infrared spectrometer produced by Bruker, model Vertex 70, with a test range of 400 cm^{-1}~4000 cm^{-1}, and the samples were prepared by the KBr pressing method.

The preparation method of the samples to be tested for FTIR test was the same as that of the XRD test specimens. First, weigh 1.5 mg of a dried solid sample and mix it with 150 mg of dried KBr powder (sample mass: KBr mass = 1:100), pour it into an agate mortar, and grind it thoroughly. After grinding, press the tablets. Test a pure KBr sample as a calibration before starting the formal test.

SEM-EDS test

SEM was utilized to examine and analyze the differences in micro-morphology of the specimens at different ratios. For this test, a Thermo Fisher (formerly FEI) Quattro s field emission ambient SEM was used to observe the micromorphology of the test specimens and the hydration products were analyzed by EDS energy spectroscopy.

The preparation method of the samples to be tested for SEM and EDS test was the same as that of the XRD test specimens.

Results

The primary factors influencing the mechanical properties of various solid waste gelling systems included the amount of CCS mixed, the Na_2SO_4 content, and the type of gelling system. The experimental program employed a fixed-variable method to systematically investigate the impact of these different factors on the mechanical properties of the gelling systems.

Compressive strength

Effect of CCS on compressive strength

CCS acted as an alkali activator in the gelling system, exerting a considerable influence on its mechanical properties. Figure 3 illustrates the compressive strength test results for specimens with varying CCS dosages and Na_2SO_4 contents, evaluated after 28 days of curing.

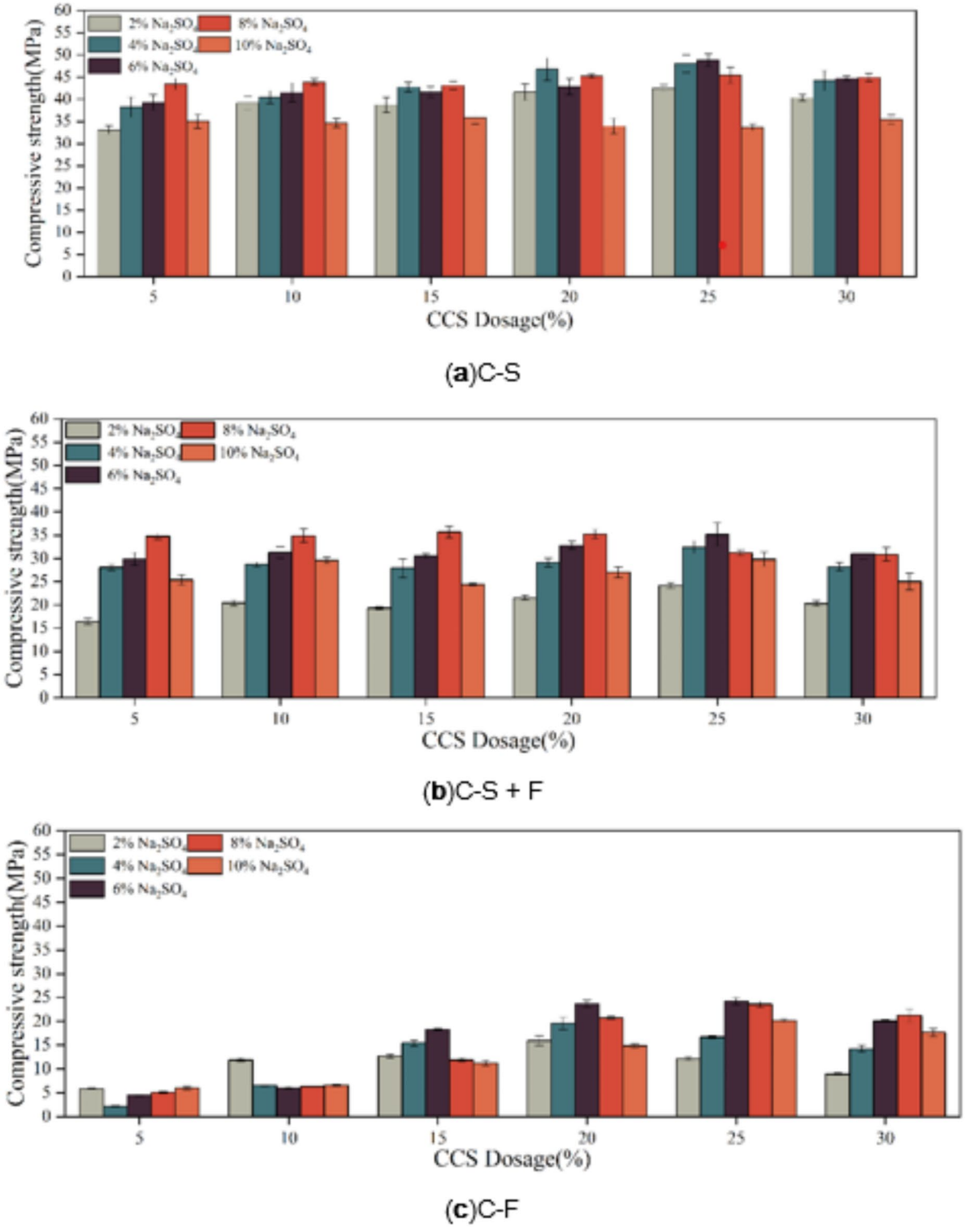

Fig. 3. Effect of CCS dosage on the mechanical strength of multi-component solid waste cementitious system. (CCS dosage of 5%, 10%, 15%, 20%, 25%, 30%). (**a**) CCS-Slag system. (**b**) CCS-Slag + FA system. (**c**) CCS-FA system.

As illustrated in Fig. 3, the compressive strength of the three gelling systems demonstrates a pattern of initial increase followed by a decline with the elevation of the CCS dosage. The majority of the samples reached their maximum strength when the CCS dosage was 25%. The C-S and C-F exhibited a pronounced influence from calcium carbide slag, with a discernible trajectory of enhanced strength. The compressive strength of the C-S increased by approximately 45%. In the C-F, when the Na_2SO_4 content is 6%, the compressive strength can be

increased from 4.5 MPa to nearly 24.2 MPa with an increase in the CCS dosage, representing a 447.78% increase. The compressive strength of the C-S + F changes more slowly, with an increase of 15–20%.

The highest compressive strength was exhibited by C-S, reaching a peak of 49.2 MPa, followed by C-S + F at 35.8 MPa. The compressive strength of C-F was found to be the lowest, reaching a peak of only 24.2 MPa.

The strength of the three cementitious systems is observed to increase with the addition of CCS, reaching a maximum at 25% CCS, when the Na_2SO_4 content is held constant. For the C-S, when the CCS dosage was low (CCS dosage % < 25%), the strength of the system increased with the Na_2SO_4 content, reaching a maximum at 8% Na_2SO_4 content. When the CCS dosage was ≥ 25%, the optimal Na_2SO_4 content was 6%.The law of the influence of Na_2SO_4 and CCS on C-S + F was the same as that of C-S, but as the content of Na_2SO_4 increased, the strength of the system increased more, indicating that the influence of Na_2SO_4 on C-S + F was more significant than that of C-S. For the C-F, when the CCS content was low (CCS dosage % < 10%), the strength of the system increased with increasing Na_2SO_4 content, and at that time, the Na_2SO_4 excitation effect dominated. As the CCS content increased, the two influencing factors jointly affected the cementitious system.

The low early strength observed in the C-F could be attributed to the poor early hydration activity of FA, which resulted in a slow hydration reaction[30,31]. However, as the Ca^{2+} and OH^- generated from CCS hydration increase, FA begin to hydrate and form cementitious compounds. The incorporation of CCS provides both Ca^{2+} and an alkaline environment, enhancing the early hydration of FA.

Slag can be rapidly decomposed in an alkaline environment, and Ca^{2+} ions released from dissolved CCS particles also promote the formation of C-(A)-S-H type gels. Therefore, the compressive strength of the C-S and C-S + F are higher than that of the C-F[32].As the amount of CCS increases, the strength of the cementitious system improves. This suggests that using CCS as an alkali activator positively impacts the strength of the cementitious system. Based on the compressive strength data for each system, a 25% CCS dosage is identified as optimal for achieving higher strength in the cementitious systems.

Effect of Na2SO4 on compressive strength

The test results indicated that the cementitious system achieved its optimal mechanical properties with a CCS dosage of 25%. In order to further investigate the effect of Na_2SO_4 content on these properties, experiments were carried out to vary the Na_2SO_4 content with the aim of exploring how different Na_2SO_4 contents affect the macroscopic mechanical properties of the cementitious system. Experimental results illustrating these effects are shown in Fig. 4.

In the C-S, the optimal Na_2SO_4 content decreases from 8 to 4% as the dosage of CCS increases. For the C-F, the optimal Na_2SO_4 content decreases from 10 to 6% as the dosage of CCS increases. In the C-S + F, the optimal Na_2SO_4 content decreases from 8 to 6% with an increase in CCS dosage. The CaO content of the Slag is 39.0%, which allows for the production of $Ca(OH)_2$ during hydration. FA contains 12.7% CaO, while the Slag-FA mixture has a CaO content of approximately 25.9%. At lower CCS dosages (≤ 15%), a higher Na_2SO_4 content is necessary to achieve effective activation. Conversely, at higher CCS dosages (> 15%), effective activation can be achieved with a lower Na_2SO_4 content. The optimal Na_2SO_4 content also depends on the CaO content in the geopolymer. Sulfate is most doped at 6% when the CCS dosage is 25%.

When the CCS content is 25%, with an increase in the Na_2SO_4 content, the compressive strength of C-S increases from 42.9 MPa to 49.2 MPa, an increase of 15.3%; the compressive strength of C-S + F increased from 24.3 MPa to 35.4 MPa, an increase of 45.7%; the compressive strength of C-F increased from 12.2 MPa to 24.2 MPa, an increase of 98.4%. The effect of sodium sulfate on the compressive strength of C-F is the most significant, followed by C-S + F, and the effect on C-S is the least. This indicated that sodium sulfate could effectively activate volcanic ash materials. The effect of activation was more pronounced for low-activity volcanic ash materials, which could significantly increase the volcanic ash activity of the material and improve utilization.

SO_4^{2-} ions react with the hydration products of the gelling system to form the AFt. Simultaneously, SO_4^{2-} ions can react with Ca^{2+} to form $CaSO_4$[33,34]. $CaSO_4$ and AFt crystals can fill the pores in the network structure of the hydration products, and this filling increases the overall compactness of the hydrated product, leading to an enhancement in its compressive strength. However, as the sulfate concentration continued to increase, the compressive strength of the material started to decrease, especially during the later stages of hydration. This decline can be attributed to two factors: first, as the reaction progresses, some Na_2SO_4 crystals are consumed, which creates pores and reduces compressive strength; second, excessive SO_4^{2-} ions can cause sulfate attack on the hydration products within the gel system.

Microscopic analysis

XRD

Figure 5 displays XRD patterns of three gelling systems with CCS dosages of 5%, 25%, and 30%, and 6% Na_2SO_4 content after 28 days of curing. With increasing CCS dosage, the diffraction peaks of hydration products became notably more pronounced. This suggested that incorporating CCS creates an alkaline environment favorable for cementitious system hydration, thus accelerating the hydration reaction. Significant hydration products such as AFt, C-(A)-S-H gel, and mullite are observed in increased amounts.

As can be seen in Fig. 5, as the CCS content increased, the hydration products continued to increase, and diffraction peaks of $Ca(OH)_2$ and $CaCO_3$ appeared at the same time, indicating that CCS hydration produced excess $Ca(OH)_2$, which reacted with CO_2 to form $CaCO_3$. A comparison of the three gelling systems showed that as the CCS dosage increased, the $Ca(OH)_2$ diffraction peak in C-S was relatively stronger, and the $Ca(OH)_2$ diffraction peak in C-F was relatively weaker, indicating that a larger amount of $Ca(OH)_2$ was consumed during the hydration of FA, and the effect of CCS dosage was more significant in C-F. This could also be seen from the change in the diffraction peak of Na_2SO_4. As the CCS content increased, the diffraction peak of Na_2SO_4 decreased, indicating that Na_2SO_4 was consumed and the hydration product AFt was formed.

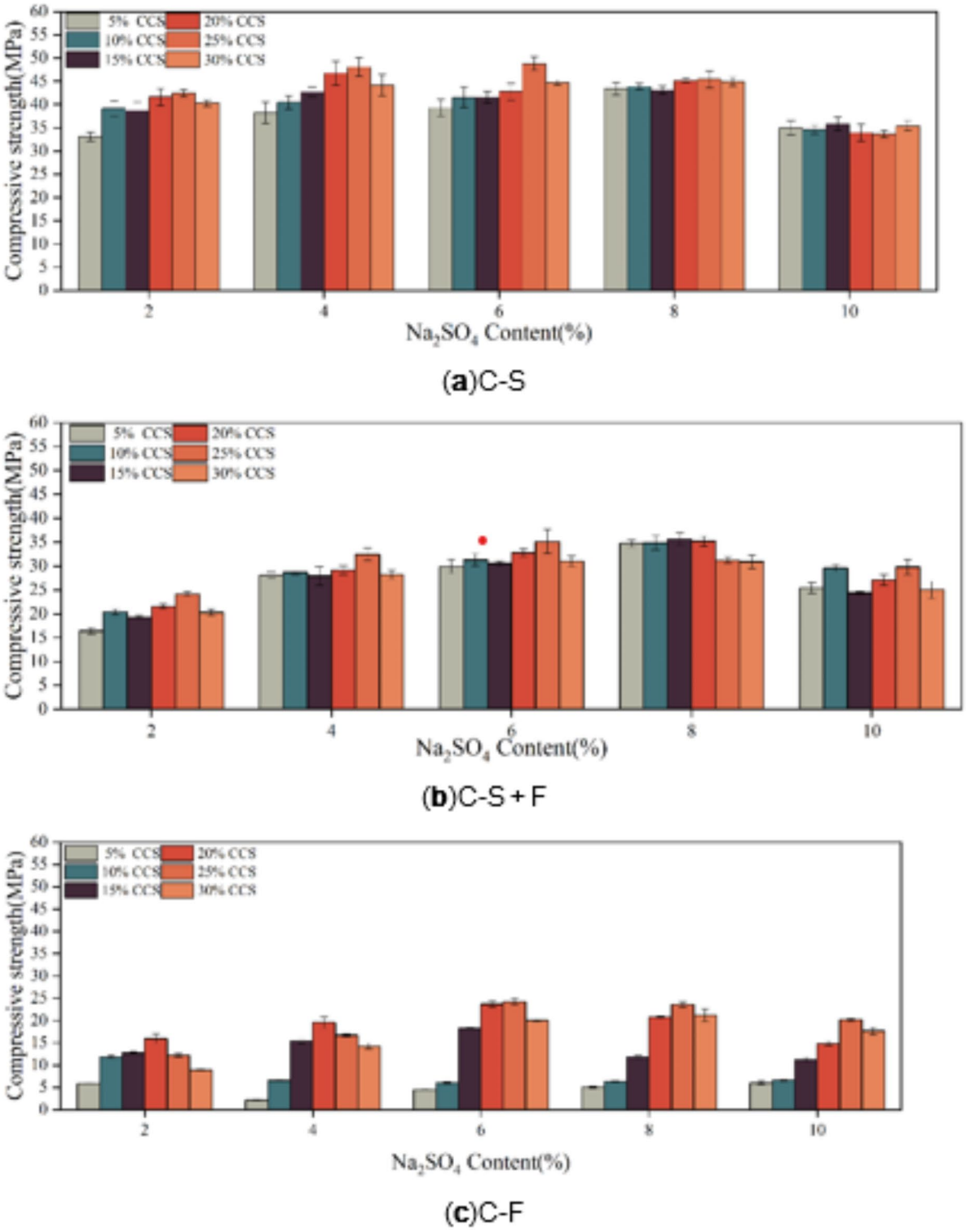

Fig. 4. Effect of Na_2SO_4 dosage on the mechanical strength of multi-component solid waste cementitious system. (Na_2SO_4 dosage of 2%, 4%, 6%, 8%, 10%). (**a**) CCS-Slag system. (**b**) CCS-Slag + FA system. (**c**) CCS-FA system.

Figure 6 showed the XRD patterns of samples with different gelling systems with a CCS content of 25%, which were kept unchanged for 28 days and had different Na_2SO_4 contents. As could be seen in Fig. 6, when the Na_2SO_4 content was 2%, the products in the three systems were C-(A)-S-H, $Ca(OH)_2$, and a small amount of AFt. As the Na_2SO_4 content increased, the AFt diffraction peak increased and the amount of AFt generated increased. When the Na_2SO_4 content was 10%, the hydration product contained more obvious $CaSO_4$, and a

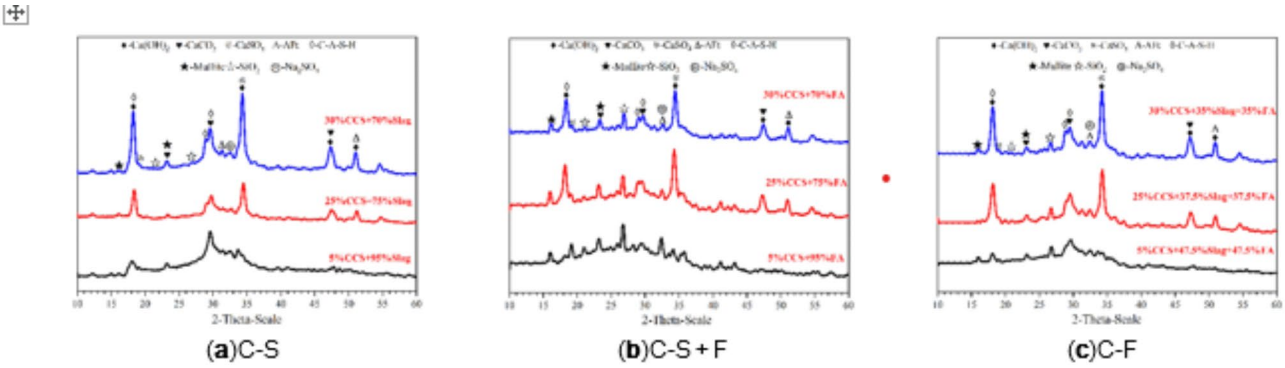

Fig. 5. XRD comparison of different cementitious systems with 5%, 25%, and 30% CCS dosage. (**a**) CCS-Slag system.
(**b**) CCS-Slag + FA system. (**c**) CCS-FA system.

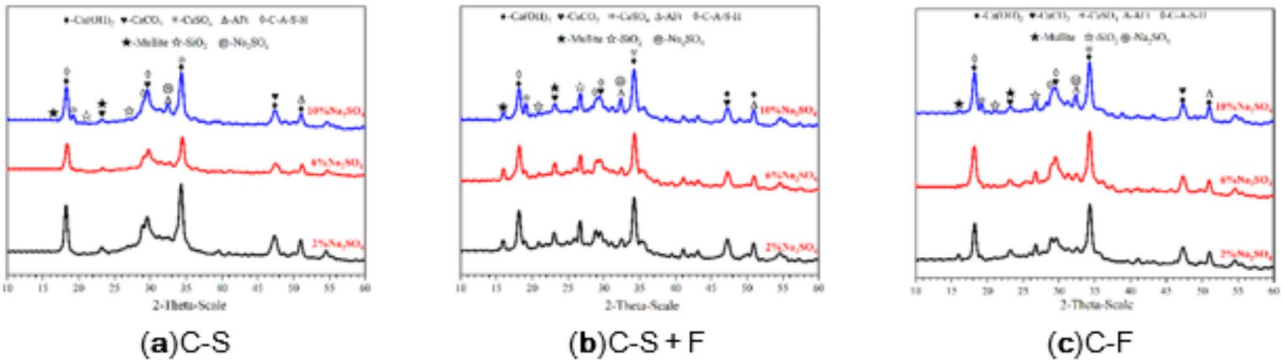

Fig. 6. XRD images of different cementitious systems at 2%, 6% and 10% Na_2SO_4 contents. (**a**) CCS-Slag system (**b**) CCS-Slag + FA system. (**c**) CCS-FA system.

large amount of $CaSO_4$ was produced. Figure 6a showed that when the Na_2SO_4 content was increased from 2–6%, the diffraction peaks corresponding to $Ca(OH)_2$[35] decreased significantly, while the peaks associated with the C-(A)-S-H gel[36] increased correspondingly, and the diffraction peaks corresponding to AFt also increased slightly. When the Na_2SO_4 content was increased to 10%, a distinct diffraction peak of Na_2SO_4 was observed, indicating that excess Na_2SO_4 crystals precipitated and the $CaSO_4$ product also increased. Figure 6b showed that as the Na_2SO_4 content increased, the $Ca(OH)_2$ diffraction peak weakened, while the diffraction peaks of the hydration products increased. This indicated that sulfate had a positive effect on the hydration of both monocomponent and composite cementitious systems. Figure 6c showed a similar trend, where an increase in Na_2SO_4 content led to a decrease in the $Ca(OH)_2$ diffraction peak and an increase in the C-(A)-S-H gel peak and the AFt diffraction peak, and a new product, mullite, appeared. This showed that sulfate promoted the hydration reaction. When the Na_2SO_4 content reached 10%, diffraction peaks of both crystalline Na_2SO_4 and gypsum appeared, reflecting changes in the hydration products. Overall, the right amount of sulfate promoted the hydration reaction, but excess sulfate not only precipitated crystals that hindered the hydration process, it also formed gypsum and other low-strength products, which adversely affected the strength of the cementitious system.

FTIR

Figure 7 shows the FTIR plots of specimens cured for 28 days at 5% CCS and 25% CCS for the three cementitious systems. Where the low wave number region (450 cm^{-1}-820 cm^{-1}) was the bending vibration of Si-O-Si (451 cm^{-1}) and Si-O-Al (619 cm^{-1})chemical bonds in Slag and FA[37,38], it could be seen that along with the increase of the dosage of CCS, the low-band transmittance in the C-S and C-F increases significantly. It shown that increasing the dosage of CCS could accelerate the hydration rate of Slag and FA, which was consistent with the compressive strength results. The strong absorption peak in the middle wave number region (820 cm^{-1}-1200 cm^{-1}) belonged to the hydration product C-(A)-S-H (Si-O-Si(Al) (962 cm^{-1}))[39] of the gelling system, and the appearance of this peak characterized the production and transformation of C-(A)-S-H, and the C-F showed a significant difference, indicating that the CCS can effectively stimulate the FA for hydration reaction. In addition, analysis of Fig. 7 shown that the Si-O-Si(Al) (962 cm^{-1}) of C-S absorption peak was narrow and sharp, indicating that the hydration product had a high degree of polymerization of silica-aluminate ions, and generates more and denser C-(A)-S-H, which was the reason for the highest compressive strength of the C-S.

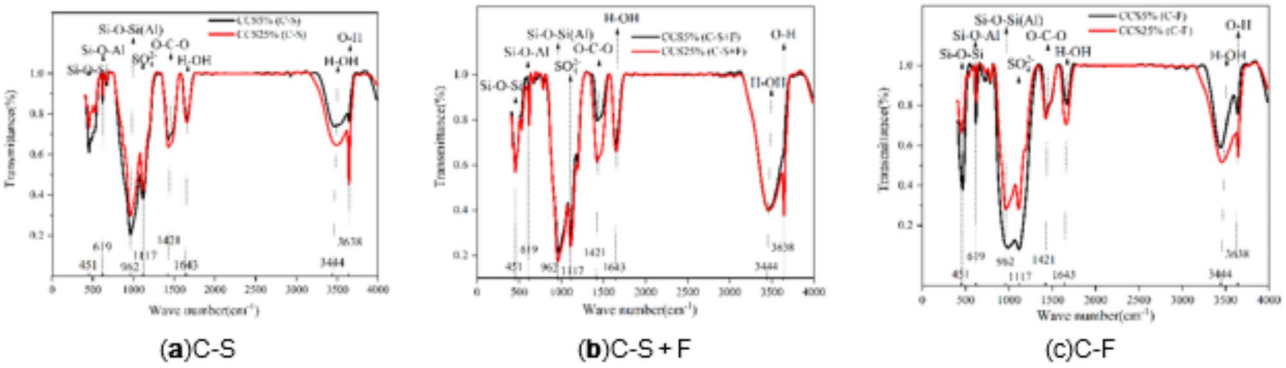

Fig. 7. FITR of 5% and 25% CCS dosing for different cementitious systems. (**a**) CCS-Slag system. (**b**) CCS-Slag + FA system. (**c**) CCS-FA system.

At the same time, the absorption peak of SO_4^{2-} appeared around the wave number of 1117 cm^{-1} [40], indicating that sulfate existed in the gelling system at this time. The absorption peak near 1420 cm^{-1} was the characteristic peak of O-C-O[41] chemical bonding of CO_3^{2-}, indicating carbonization of the hydration product $Ca(OH)_2$. The absorption peaks with wave numbers near 1643 cm^{-1} and 3444 cm^{-1} were characteristic peaks of H-OH bonding indicating the presence of bound water in the product[42]. The presence of these bands was due to crystalline H_2O in C-(A)-S-H structure. The absorption peak with wave number near 3638 cm^{-1} was the peak characterizing the O-H chemical bond in $Ca(OH)_2$, which increases along with the increase in the dosage of CCS, indicating that CCS provides an alkaline environment for the gelling system, which was in agreement with the XRD analysis.

In conclusion, CCS effectively boosted the hydration of both slag and FA. The FTIR spectra of the six samples shown similar wave forms, indicated fundamental consistency in hydration products among the three systems. Differences in compressive strength were attributed to variations in hydration product polymerization degree rather than differences in product type.

SEM and EDS

Figure 8 shows the SEM images of three gelling systems with 5%, 25% and 30% CCS added at 6% Na_2SO_4 content during 28 days of maintenance. As shown in Fig. 8a, b, the addition of CCS accelerated the hydration reaction, with the amount of CCS increased from 5 to 25%, more hydration products were generated, cemented and stacked with each other, and the micro structure shown a dense state. When the dosage of CCS exceeds 25% and reaches 30%, as shown in Fig. 8b, c, and the original hydration products are replaced by a large number of foil-like products, which generates a part of the hollow structure and reduces the compressive strength[43]. The microscopic results were consistent with the experimental data, confirming that the moderate amount of CCS dosing on the C-S was favorable, and shown a first increase and then decrease in the law, in 25% to achieve the best results.

As illustrated in Fig. 8d, with a lower dosage of CCS, the pore spaces within the cementitious system contained numerous unhydrated spherical FA particles. At this stage, only a minimal degree of FA had reacted, producing a limited amount of hydration producted that partially fill the pore spaces, resulting in relatively low compressive strength. As the CCS dosage increased to 25%, the spherical FA particles are nearly absent. The hydration reaction of FA generated an amorphous C-(A)-S-H gel, which, along with unhydrated gelling material particles, cements together to form a denser microstructure. This transition corresponded to a significant increase in compressive strength. However, when the CCS dosage was further increased to 30%, as shown in Fig. 8f, the previously dense microstructure is largely replaced by inter-stacked flakes and rods. This change leads to the formation of a more open, grid-like structure, resulting in a decrease in compressive strength.

Analyzing Fig. 8g, at this dosage, the microstructure of the cementitious system exhibits a small proportion of C-(A)-S-H gel that encapsulates unhydrated FA and Slag powder. Spherical unhydrated FA particles remain visible within the microstructure, which otherwise appears relatively dense. However, the presence of cracks is noticeable. Upon increasing the dosage of CCS to 30%, as depicted in Fig. 8h, i, the cementitious material undergoes significant hydration. A substantial amount of hydration products fills the pore spaces; however, the emergence of needle-like and rod-like structures within these products disrupts the previously dense microstructure. This disruption results in a more open, loose morphology, and the development of additional cracks, which contributes to a reduction in compressive strength.

Figure 9 shows the SEM images of specimens of three cementitious systems with 25% CCS and 2%, 6% and 10% Na_2SO_4 content, respectively, which were cured for 28 days. Figure 9a illustrates that in the C-S with 2% Na_2SO_4 content, there are numerous flaky $Ca(OH)_2$ crystals and a small amount of $CaCO_3$. As the Na_2SO_4 content increases to 6%, the flaky $Ca(OH)_2$ is largely replaced by hydrated gel, resulting in a denser microstructure. At 10% Na_2SO_4 content, the microstructure shows the formation of gypsum clusters and a significant amount of Na_2SO_4 crystals on the surface of the hydration products. These Na_2SO_4 crystals absorb moisture, expand, and compromise the structural stability of the cementitious system. Figure 9d shows that with 2% Na_2SO_4 content in the C-F filamentous flocculent products appear on the surface of the FA particles, indicating a weak hydration reaction. As Na_2SO_4 content increases, the hydration of the FA particles progresses,

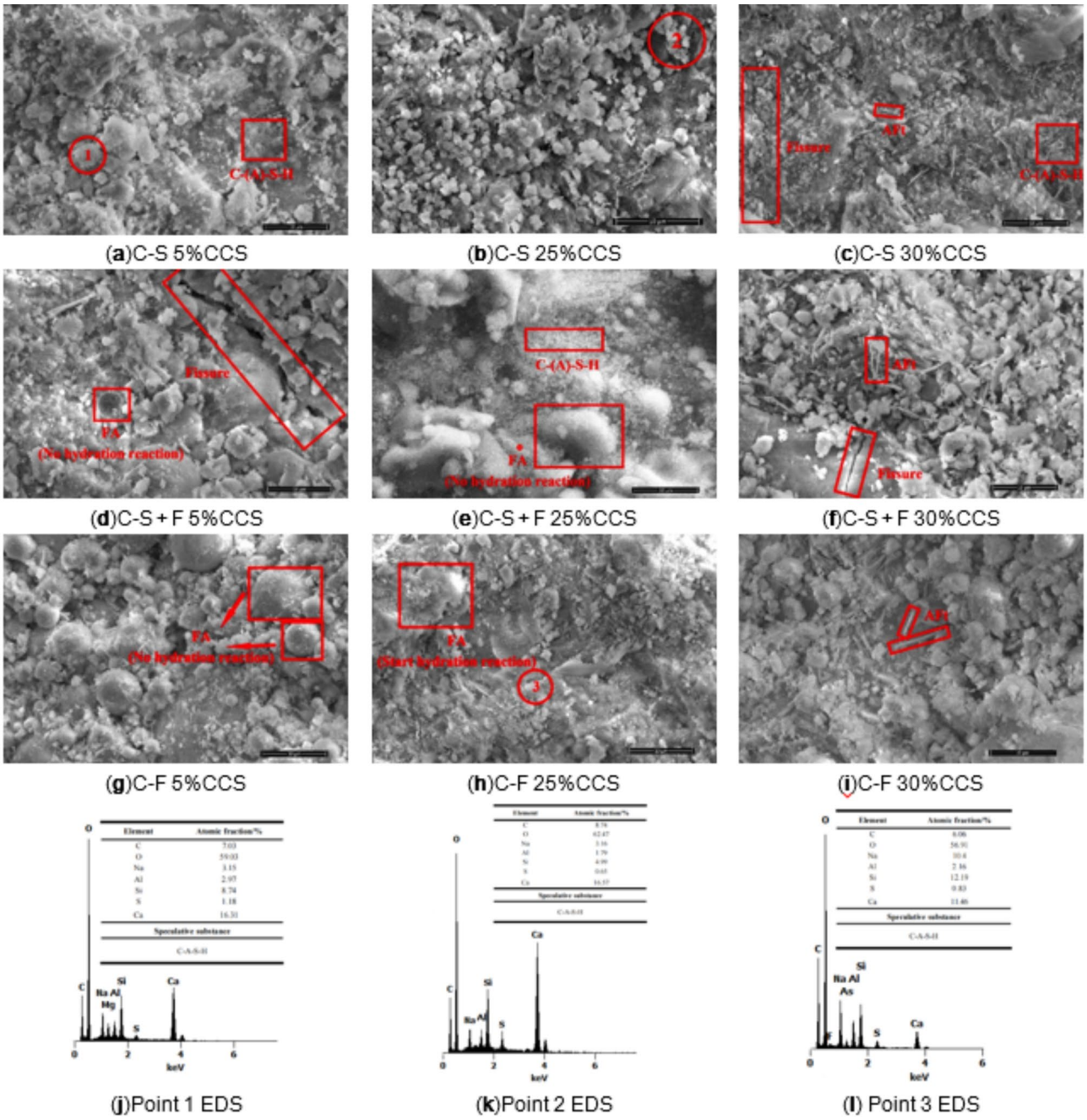

Fig. 8. SEM images of the gelling systems with 5%, 25% and 30% CCS dosage. (6% Na_2SO_4 content). (**a**) CCS-Slag system (5% CCS dosage). (**b**) CCS-Slag system (25% CCS dosage). (**c**) CCS-Slag system (30% CCS dosage). (**d**) CCS-Slag + FA system (5% CCS dosage). (**e**) CCS-Slag + FA system (25% CCS dosage). (**f**) CCS-Slag + FA system (30% CCS dosage). (**g**) CCS-FA system (5% CCS dosage). (**h**) CCS-FA system (25% CCS dosage). (**i**) CCS-FA system (30% CCS dosage). (**j**) EDS mapping of point (1) (**k**) EDS mapping of point (2) (**l**) EDS mapping of point 3.

with the resulting hydrated C-(A)-S-H gel enveloping the unhydrated FA particles and forming a dense matrix that fills the pores. At 10% Na_2SO_4 content, numerous rod-like and granular products appear, accompanied by the formation of cracks, which indicates damage to the cement structure. Figure 9h, i reveal that at 10% Na_2SO_4 content, the microstructure is characterized by a high density of needle-like and rod-shaped products, alongside an increase in porosity. The various hydration products are scattered and fail to bond effectively, leading to severe structural damage.

The $Ca(OH)_2$ in the CCS provided Ca^{2+} and OH^- ions. Na_2SO_4 contributes Na^+ ions and SO_4^{2-} ions, which reacted to form NaOH. This NaOH, in turn, interacted with Slag and FA to produce additional hydration products such as C-(A)-S-H, which filled the pores, optimize pore structure, and improve compressive strength.

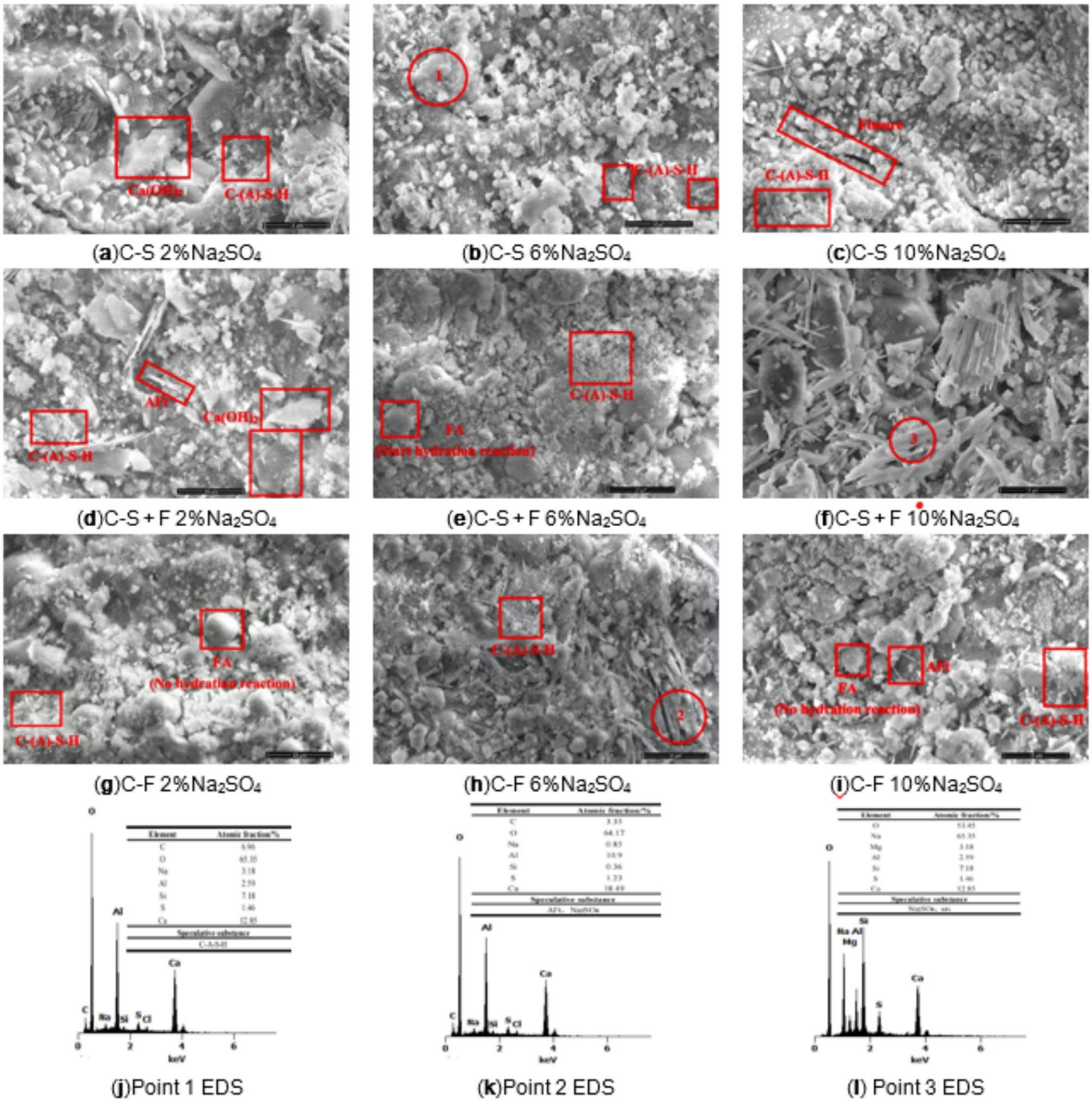

Fig. 9. SEM images of gelling system at 2%, 6% and 10% Na_2SO_4 content. (25% CCS dosage). (**a**) CCS-Slag system (2% Na_2SO_4 content). (**b**) CCS-Slag system (6% Na_2SO_4 content). (**c**) CCS-Slag system (10% Na_2SO_4 content). (**d**) CCS-Slag + FA system (2% Na_2SO_4 content). (**e**) CCS-Slag + FA system (6% Na_2SO_4 content). (**f**) CCS-Slag + FA system (10% Na_2SO_4 content). (**g**) CCS-FA system (2% Na_2SO_4 content). (**h**) CCS-FA system (6% Na_2SO_4 content). (**i**) CCS-FA system (10% Na_2SO_4 content). (**j**) EDS mapping of point (1) (**k**) EDS mapping of point (2) (**l**) EDS mapping of point 3.

However, excessive Na_2SO_4 leads to the formation of more Aft and the precipitation of Na_2SO_4 crystals, which expand and damage the pore structure, ultimately reducing compressive strength. Similarly, an excess of CCS may result in unreacted $Ca(OH)_2$ precipitating as crystals, which weakens the crystal connection layer and decreases compressive strength.

Compressive strength prediction model based on projection-seeking regression PPR model

$$f(x) = E(Y_i | X_1, X_2, X_3 \cdots, X_P) = \bar{y}_i + \sum {}_{m=1}^{M} \beta_m f_m \left(\sum {}_{j=1}^{P} \alpha_{jm} x_j \right) \quad (1)$$

Slag dosage (%)	Na_2SO_4 content (%)	FA Dosage (%)	CCS Dosage (%)
1.000	0.420	0.407	0.322

Table 3. Impact weights of the respective variables of the PPR model.

Sample type	Number of samples	Qualification rate (%)	Average relative error (%)
Training samples (T)	60	81.67	10.47
Reserved samples (R)	20	85.00	5.98

Table 4. Qualification rate and relative error between calculated value and test data based on PPR model.

PPR can objectively analyze and describe the structural characteristics and laws of each data sample, and achieve high-precision simulation calculations without making any assumptions based on the data information of each factor[44]. This method employs computer technology to project multi-dimensional spatial data into a low-dimensional subspace. By minimizing a specific projection index, it identifies a projection that captures the underlying laws and characteristics of the original data, facilitating the analysis of multi-dimensional datasets[45]. Let there be a set of random variables (X, Y), where Y is a Q-dimensional random variable. X is a P-dimensional random variable. PPR can be based on the results of n observations of (X, Y) (Xi, Yi) (i = 1,2,3,…,n). The model X, Y PPR can be expressed as follows: the regression function f (x) = E (Y | X = x) is approximated in the form of a weighted sum of multiple ridge functions:

Where: f_m -mth ridge function; M -upper limit of the number of ridge functions; β_m -ridge function contribution weight coefficient; α_{jm} -mth projection value in the jth direction(j = 1, 2, 3, ···,M); $\sum_{j=1}^{P} \alpha_{jm}^{2} = 1$

Minimization criteria:

$$L_2 = \sum_{i=1}^{Q} W_i E\left[Y_i - EY_i - \sum_{m=1}^{M_u} \beta_m f_m \left(\sum_{j=1}^{P} \alpha_{jm} X_j\right)^2\right] = min \tag{2}$$

Where: M_u -optimal number of ridge functions; W_i -weight coefficient of the dependent variable[46].

PPR projects multidimensional data to a lower dimension, gradually optimizes, iteratively calculates in hierarchical groups, and thereby calculates the ridge function f_m, the optimal number of ridge functions m_u, the projection direction α_{jm} and the weight coefficient w_i of each factor, determines the regression function, and thereby makes L_2 satisfy the minimum value. For details of the basic principles and theories of PPR, see the literature[44].

Compressive strength prediction model

The PPR model was developed by training the compressive strength data for different CCS dosage, Na_2SO_4 content and cementitious systems using the methodology presented in Sect. 3.3.1. The established predictive model was then used to fit the model samples, and the accuracy of the predictive model was assessed by analyzing the differences between the anticipated values and the samples. Nevertheless, the model's expected values did not quite match its inherent advantages and disadvantages. As a result, as Table A shows, the test data was split into training and retention samples. The model's accuracy is validated by predicting values for the retained samples using simulated training data. From the table, it can be seen that the independent variables are CCS dosage (X_1), Slag dosage (X_2), FA dosage (X_3) and Na_2SO_4 content (X_4), and the predictor is compressive strength (Y_1). The model parameters were configured as follows: $P = 4$, $Q = 1$, $N = 60$, $M = 5$, $Mu = 3$, and $Span = 0.2$. Table 3 presents the influence weights of variables after constructing the PPR model. Here, P denotes the count of independent variables, Q represents the number of dependent variables, and N signifies the training sample size. M and Mu denote the maximum number of ridge functions and the optimal number of ridge functions, which are crucial for improving the prediction accuracy. Span refers to the smoothing coefficient, which ranges from 0 to 1.0, influencing the model's sensitivity; lower values indicate heightened sensitivity[47].Since the parameter values of the PPR model are objectively verifiable, the problem of non-uniqueness of the model caused by manual parameter assignment is avoided.

PPR model precision analysis

The precision of the PPR model was assessed using a 15% threshold for relative error between calculated and test values. Samples were considered qualified if their relative error was below 15%. Table 4 displays qualification rates and average relative errors for modeled and tested samples. The model demonstrates excellent fit with test data, showing robust stability and high accuracy in predicting compressive strength across various mixing ratios.

Contour plots based on the PPR model show the effect of CCS dosage, Slag dosage, FA dosage and Na_2SO_4 content on the compressive strength of the different cementitious systems as shown in Fig. 10. The PPR theory can be used to determine the effects of CCS dosage and Na_2SO_4 content on the compressive strength of the three cementitious systems, providing a feasible method for proportioning design and mechanical strength prediction of all-solid waste cementitious systems.

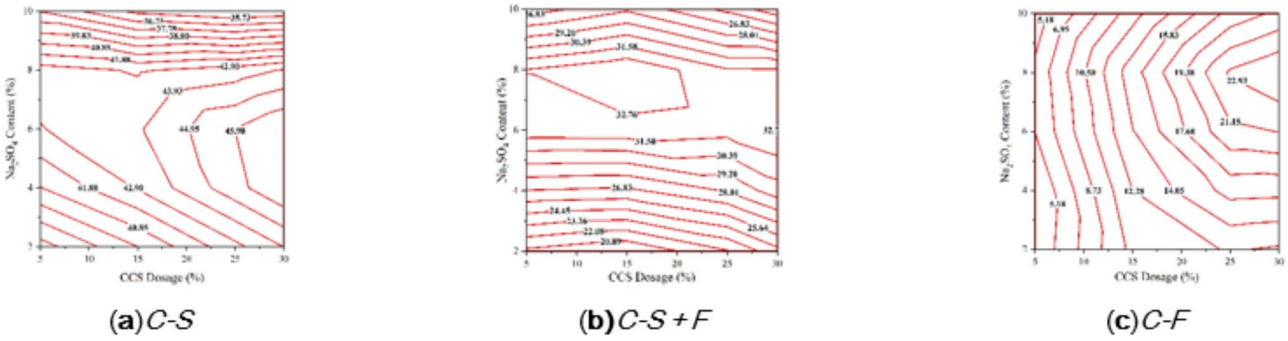

Fig. 10. PPR compressive strength prediction contour plot. (**a**) CCS-Slag system. (**b**) CCS-Slag + FA system. (**c**) CCS-FA system.

Conclusions

In this paper, the preparation of CCS-sulfate-geopolymer composite cementitious system, the study of CCS, Na_2SO_4 on the mechanical properties of the composite cementitious system, the establishment of the composite cementitious system 28d strength prediction model. The main conclusions are as follows:

1. CCS and Na_2SO_4 have a great influence on the mechanical properties of the composite cementitious system, the optimum dosage of CCS is 25% and the optimum content is 6%. CCS and Na_2SO_4 have the most significant stimulating effect on the C-F system.
2. The CCS provides alkaline environment as well as Ca^{2+} for the hydration reaction of the cementitious system, which provides sufficient conditions for the hydration reaction of geopolymer, and accelerates the rate of hydration reaction. When the dosage of CCS exceeds 25%, a large number of $Ca(OH)_2$ saturated precipitation, precipitated $Ca(OH)_2$ crystals filled in the gel, destabilizing the gel, forming part of the stress weak zone, resulting in a reduction of compressive strength.
3. The mechanical effect of Na_2SO_4 content on the gel system is divided into two stages: Na_2SO_4 content is less than < 6%, Na_2SO_4 and geopolymer hydration products react to form AFt, filling the pores and improving the strength of the gel system; Na_2SO_4 content > 6%, react with Ca^{2+} to form gypsum, and there is precipitation of Na_2SO_4, and these expansion products destroy the microstructure of the gel system, affecting the mechanical properties of the gel system.The test results showed that the idea of "turning danger into safety" was feasible.
4. Based on PPR theory, a strength prediction model of cementitious composite system was established. Practice has proved that PPR can be used to determine the 28d compressive strength of cementitious composite system at different dosages of CCS, Na_2SO_4, Slag and FA, which provides a feasible method for designing and predicting the strength of cementitious composite materials with different ratios.

Data availability

The datasets generated during and/or analysed during the current study are available from the corresponding author on reasonable request.

Received: 19 November 2024; Accepted: 24 January 2025
Published online: 29 January 2025

References

1. Haddad, R. H. & Alshbuol, O. Production of geopolymer concrete using natural pozzolan: A parametric study. *Constr. Building Mater. J.* **114**, 699–707 (2016).
2. Li, L. Mitigation of China's carbon neutrality to global warming. *Nat. Commun. J.* **13**(1), 5315 (2022).
3. Qaidi, S. M., Dinkha, Y. Z., Haido, J. H., Ali, M. H. & Tayeh, B. A. Engineering properties of sustainable green concrete incorporating eco-friendly aggregate of crumb rubber: A review. *Clean. Prod. J.* **324**, 129251 (2021).
4. Gökçe, H. S., Tuyan, M. & Nehdi, M. L. Alkali-activated and geopolymer materials developed using innovative manufacturing techniques: A critical review. *Constr. Building Mater. J.* **303**, 124483 (2021).
5. Sharma, V., Dash, S. & Gupta, P. Comprehensive review of fly ash: Environmental impact and applications. *Environ. Qual. Manage. J.* **34**(2), e22338 (2024).
6. Peng, W., Xianjun, L., Shugang, H. & Lei, Z. Research progress on the activation of the cementitious properties of granulated blast furnace slag. *Metal Mine (in Chinese) J.* **10**, 157–161 (2012).
7. Jun, C., Xiaoying, J., Yuxiao, Z. & Liang, L. Phase evolution and quantitative analysis of fly ash-cement mortar in sulfate-chloride environment. *Mater. Rep. (in Chinese) J.* **22**, 161–167 (2024).
8. Rashad, A. M., Bai, Y., Basheer, P. A. M., Milestone, N. B. & Collier, N. C. Hydration and properties of sodium sulfate activated slag. *Cem. Concrete Compos. J.* **37**, 20–29 (2013).
9. Wu, P., Liu, X., Liu, X., Zhang, Z. & Wei, C. Effect of Industrial byproduct gypsum on the mechanical properties and stabilization of hazardous elements of cementitious materials. *Rev. Mater. J.* **17**(17), 4183 (2024).
10. Huang, S. Y., Li, Z. H. & Cheng, J. P. Reaction kinetics in the FA-$Ca(OH)_2$-H_2O system. *J. Chin. Ceramic Soc. J.* **14**(1), 191–197 (1986).
11. Lin, X. Q., Wang, D. M., Xu, C. Y., Zhao, J. H. & Han, F. H. Effect of sulfate and chloride exciters on FA activity. *Coal Ash J.* **24**(1), 4–7 (2012).

12. Peng, R. Design and performance study of tailings filler prepared from sodium sulfate-inspired cementitious materials. *Wuhan University of Technology. D.* Wuhan, China (2019).
13. Wei, J. & Chun, H. Mechanical properties of sisal fiber-reinforced fly ash cement mortar activated by sodium sulfate. *Constr. Building Mater. J.* **445**, 137925 (2024). ISSN 0950 – 0618.
14. Yu, Z. et al. Preparation and microscopic characteriz-ation of typical sulfate solid waste composite cementitious materials. *Inorg. Chemicals Ind. J.* **56**(04), 90–97 (2024).
15. Li, Z. Effect of alkali and sulfate on the hydration characteristic of cement-based materials containing coal gasification slag. *Mater. J.* **15**(24), 8868 (2022).
16. Huang, X. Enhancement of hydration product AFt in soft ground reinforcement. *J. Chin. Ceramic Soc. J.* **28**(4), 299–302 (2000).
17. Deng, D. H., Xiao, J., Yuan, Q., Liu, Z. Q. & Zhang, W. E. Effect of limestone powder on the sulfate erosion resistance of cementitious materials and its mechanism. *J. Chin. Ceramic Soc. J.* **10**, 1243–1248 (2006).
18. Deng, Y., Zhang, C. & Wei, X. Influence of lithium sulfate addition on the properties of Portlandcement paste. *Constr. Build. Mater. J.* **50**, 457–462 (2014).
19. Zhao, L. W., Zhu, G. Y., Li, S. P., Meng, Z. H. & Mou, X. J. Characteristics of Calcium Carbide Slag and comprehensive utilization research progress. *Clean. Coal Technol. J.* **27**(03), 13–26 (2021).
20. An, S., Wang, B. M., Chen, W. X. & Zhao, Q. X. Mechanism of action of CS to stimulate Slag-FA composite cementitious materials. *Bull. Chin. Ceramic Soc. J.* **42**(04), 1333–1343 (2023).
21. Wan, Z. H., Zhang, W. Q., Liu, Z. C. & Wang, F. Z. Study on the performance of CS-Slag composite cementitious material. *Bull. Chin. Ceramic Soc. J.* **41**(05), 1704–1714 (2022).
22. Abdelbaset, A. M., Katunský, D., Zeleňáková, M. & El-Feky, M. H. Mechanical properties stabilization of low plasticity kaolin soil using fly ash and hydrated lime. *Case Studi. Construct. Mater. J.* e03662 (2024).
23. Lam, T. V. & Nguyen, M. H. Incorporating Industrial by-products into geopolymer mortar: Effects on strength and durability. *Mater. J.* **16**(12), 4406 (2023).
24. Ling, Y. H., Xu, D. Q. & Zhao, X. H. Status and prospect of utilization of calcium carbide slag and carbon dioxide resource utilization. *Bull. Chin. Ceramic Soc. J.* **38**(09), 2876–2881 (2019).
25. Seo, J. Utilization of calcium carbide residue using granulated blast furnace slag. *Mater. J.* **12**(21), 3511 (2019).
26. Wang, Y., Huo, H., Chen, B. & Cui, Q. Development and optimization of phosphogypsum-based geopolymer cement. *Constr. Buildi. Mater. J.* **369**, 130577 (2023).
27. Feng, Y. Effects of phosphogypsum substitution on the performance of ground granulated blast furnace slag/fly ash-based alkali-activated binders. *J. Buildi. Eng. J.* **70**, 106387 (2023).
28. Li, H. Investigation on mechanical properties of excess-sulfate phosphogypsum slag cement: from experiments to molecular dynamics simulation. *Constr. Build. Mater. J.* **315**, 125685 (2022).
29. JGJ/T 70-2009; Standard for test method of performance on building mortar. *Industry Standards-Construction Industry. S.* Chinese Standard: Beijing, China, (2009).
30. Babak, V. & Ali, G. Self-healing effect of hydrogels in cement slag and fly ash pastes. *Constr. Build. Mater. J.* **438** (2024). 137036, ISSN 0950 – 0618.
31. Zhang, Y. et al. Understanding the changes in engineering behaviors and microstructure of FA-GBFS based geopolymer paste with addition of silica fume. *J. Building Eng. J.* **70**, 106450 (2023).
32. Gao, X. et al. Calcium carbide residue as auxiliary activator for one-part sodium carbonate-activated slag cements: Compressive strength, phase assemblage and environmental benefits. *Construct. Buildi. Mater.. J. Volume* **308** 125015 (2021), ISSN 0950 – 0618.
33. Lodeiroa, P. & Fernandez, J. Compatibility studies between N-A-S-H and C-(A)-S-H gels. Study in the ternary diagram Na_2O-CaO-Al_2O_3-SiO_2-H_2O. *Cem. Concr Res. j.* 41 (2011).
34. Zhao, X. Investigation into the effect of calcium on the existence form of geopolymerized gel product of fly ash based geopolymers. *Cem. Concrete Compos. J.* **103**, 279–292 (2019).
35. Shaqour, F., Ismeik, M. & Esaifan, M. Alkali activation of natural clay using a ca $(OH)_2$/Na_2CO_3 alkaline mixture. *Clay Minerals J.* **52**(4), 485–496 (2017).
36. Walkley, B. Phase evolution of C-(N)-ASH/NASH gel blends investigated via alkali-activation of synthetic calcium aluminosilicate precursors. *Cem. Concr. Res.* **89**, 120–135 (2016).
37. Mozgawa, W., Król, M., Dyczek, J. & Deja, J. Investigation of the coal fly ashes using IR spectroscopy. *Spectrochimica Acta Part. A: Mol. Biomol. Spectrosc. J.* **132**, 889–894 (2014).
38. Yu, P., Kirkpatrick, R. J., Poe, B., McMillan, P. F. & Cong, X. Structure of calcium silicate hydrate (C-S-H): Near-, mid-, and far-infrared spectroscopy. *J. Am. Ceramic Soc. J.* **82**(3), 742–748 (1999).
39. Yousuf, M., Mollah, A., Hess, T. R., Tsai, Y. N. & Cocke, D. L. An FTIR and XPS investigations of the effects of carbonation on the solidification/stabilization of cement based systems-Portland type V with zinc. *Cem. Concrete Res. J.* **23**(4), 773–784 (1993).
40. Xia, M., Yao, Z., Ge, L., Chen, T. & Li, H. A potential bio-filler: the substitution effect of furfural modified clam shell for carbonate calcium in polypropylene. *J. Compos. Mater. J.* **49**(7), 807–816 (2015).
41. Chu, D. H. CO_2 mineralization into different polymorphs of CaCO3 using an aqueous-CO2 system. *Rsc Adv. J.* **3**(44), 21722–21729 (2013).
42. Li, W. & Yi, Y. Use of carbide Slag from acetylene industry for activation of ground granulated blast-furnace slag. *Constr. Build. Mater. J.* **6**, 238 (2020).
43. Bai, Y., Guo, W. & Zhang, Y. Low carbon binder preparation from Slag-red mud activated by MSWI FA-carbide Slag: Hydration characteristics and heavy metals' solidification behavior. *J. Clean. Prod. J.* **134007** (2022).
44. Zheng, Z. G., He, J. X. & Gong, J. W. Projection pursuit regression for complex systems without assumed modeling techniques and application examples. *China Water Power Press. J. China* pp.**43** (2019).
45. Yang, H. H., Yang, W. & Liu, H. L. Fitting the stress-strain law of gravel based on PPR data modeling technology. *Mater. Rep. J.* **37**(13), 1–13 (2023).
46. Zhu, X., Bai, Y., Chen, X., Tian, Z. & Ning, Y. Evaluation and prediction on abrasion resistance of hydraulic concrete after exposure to different freeze-thaw cycles. *Constr. Building Mater. J.* **316**, 126055 (2022).
47. Nath, P. & Sarker, P. K. Effect of GGBFS on setting, workability and early strength properties of fly ash geopolymer concrete cured in ambient condition. *Constr. Building Mater. J.* **66**, 163–171 (2014).

Author contributions

Conceptualization, M. G. and Y. W.; Data curation, A. S.; Formal analysis, A. S.; Funding acquisition, M. G.; Methodology, A. S. and H. L.; Software, A. S. and Y. W.; Supervision, M. G.; Validation, H. L. and R. H.; Writing – original draft, A. S.; Writing – review & editing, M. G. and Y. W. All authors reviewed the manuscript.

Funding

This research was funded by: 1.Natural Science Foundation of Xinjiang Uygur Autonomous Region (2022D01B98). 2. Xinjiang Key Laboratory of Hydraulic Engineering Security and Water Disasters Prevention (ZDSYS-JS-2021-01). 3. "Xinjiang Key Laboratory of Hydraulic Engineering Safety and Water Disaster Preven-

tion" open project (6660946/2522GCCRC).

Declarations

Competing interests
The authors declare no competing interests.

Additional information
Supplementary Information The online version contains supplementary material available at https://doi.org/10.1038/s41598-025-88194-y.

Correspondence and requests for materials should be addressed to M.G.

Reprints and permissions information is available at www.nature.com/reprints.

Publisher's note Springer Nature remains neutral with regard to jurisdictional claims in published maps and institutional affiliations.